STRUCTURAL AND SUBSTRUCTURAL PROPERTIES OF THE ZINC AND CADMIUM CHALCOGENIDES THIN FILMS (A REVIEW)

C.J. Panchal[1], **A.S. Opanasyuk**[2], **V.V. Kosyak**[2], **M.S. Desai**[1], **I.Yu. Protsenko**[2]

[1] M.S. University of Baroda, Applied Physics Department, Faculty of
  Technology and Engineering,
  Vadodara, 390001, Gujarat, India
  E-mail: cjpanchal_msu@yahoo.com

[2] Sumy State University,
  2, Rimsky-Korsakov Str., 40007, Sumy, Ukraine
  E-mails: opanasyuk_sumdu@ukr.net, protsenko@aph.sumdu.edu.ua

In this paper, the structural properties of the zinc and cadmium chalcogenide thin films are considered. The influence of the structural defects such as grain boundaries, dislocations, native point defects, etc., on the optical and electrical properties of the thin films was studied. The methods of the II-VI thin films deposition are described. The influence on the sub-structural properties (phase compositions, texture, grain size, stacking faults concentration, micro deformation levels, and coherent domain size) of the thin films grown by the close-spaced vacuum evaporation method was analyzed. The growth conditions of the thin films with optimized parameters have been determined.

1. INTRODUCTION

Rapid progress in microelectronics strongly depends on the development and application of the new semiconductor materials. The first semiconductor materials for microelectronics devices were germanium and silicon. The basic elements of the microelectronics such as diodes and transistors were based on these materials [1-3]. In the following year's semiconductor lasers, tunnel diodes, Gann diodes, and optical modulators, the III-VI compounds have found wide applications. Nowadays the technologies of manufacturing single crystals and thin films of these compounds have been studied very well and a range of devices based on such compounds is already in use in industry [4]. Among novel semiconductor materials the II-VI compounds based on elements of the II group (Cd, Zn, Hg) and VI group (O, S, Se, Te) can be considered as the most important and promising. Their unique properties, which allows them to be used in different optical, acoustical, electronic, optoelectronic, nuclear physics devices, etc., can explain the strong interest in II-VI compounds [5-8]. All chalcogenides are direct energy band gap semiconductors with a band gap (BG) from hundredth part of the eV (for mercury chalcogenides) to $E_g = 3.68$ eV (for ZnS). It allows spectral range from 300 nm to about 2000 nm in II-VI based photoelectronics devices. The crystal structure of the II-VI materials viz. Cubic or Hexagonal

has no center of symmetry that can cause strong piezoelectric effect. In addition, hexagonal crystals have pyroelectric properties. It can be used for manufacturing different detectors, acousto-electronic amplifier, and strain sensor, etc. [5-7]. High density of some compounds (CdTe, ZnTe, CdSe) makes it possible to use such materials as detectors of hard and α - radiation [8-9]. It should be noted that the reciprocal solubility is typical for II-VI materials. Thus, one can create novel materials with predicted band-gap, lattice parameter, and the range of transmission spectral, etc. [10].

Polycrystalline and epitaxial films of II-VI semiconductor compounds have drawn scientists' attention for more than four decades [11-12]. Such attention is related to the possibility of creation of high-performance electronic devices based on these thin layers. However, at the same time, in most cases expectations of researchers remain unsatisfied. It is largely conditioned by the structural specialty of chalcogenide thin films, which, in turn, determine the electro-physical and optical properties of the films. The basic requirements demanded for thin films are close to stoichiometry chemical composition, single-phase and textured columnar structure, with low concentration of stacking fault defects (SFD), and growth twins [13].

However, a plenty of research work on II-VI thin films is required to resolve complex technological problems. Among them: high deviation from stoichiometry, co-existence of two polymorphic phase viz. zinc-blende (ZB) and wurtzite (WZ), high concentration of SFD and growth twins, high level of microstresses and macrostresses, a tendency for anomalous axial textures formation, etc. [12, 14-15]. The high level of the structural defects, which can be recombination centers and deep traps, can deteriorate the electrical properties of the layers. Thus, the creation of the thin films with predicted properties is connected with the control of defect structure.

In this paper the peculiarities of II-VI compounds thin film formation that have a strong effect on the main electrical and optical properties are considered. We devote a special attention to the zinc and cadmium chalcogenides thin films obtained by the close-spaced vacuum sublimation method.

2. THE PECULIARITIES OF CRYSTAL STRUCTURE FORMATION OF THE ZINC AND CADMIUM CHALCOGENIDES SINGLE-CRYSTAL AND THIN FILMS

2.1 Some structural and physical properties of the chalcogenide compounds

Zinc and cadmium chalcogenides are direct energy band gap semiconductors with BG from $E_g = 1.46$ eV (CdTe) to $E_g = 3.68$ eV (ZnS). The hybrid ion-covalent bond with prevalence of the covalent component is typical for these materials. The possibility of controlling the electrical properties of the chalcogenides depends on the homogeneity of the regions in the films. The homogeneity regions have unsymmetrical shape and, as a rule, locate in metal or chalcogenide-excess region. As a result, only undoped CdTe with either n-or p-type conductivity can be obtained. ZnTe always have p-conductivity, the rest of the materials have n-conductivity [7, 10, 12, 16, 17]. However, some published results are in contradiction to this. For example, in papers [18-19] the ZnSe and CdSe single crystal with p-type of conductivity was obtained by the annealing of chalcogenides samples under excess of pressure.

All chalcogenides have rather high temperature of the melting point (1370 K – CdTe, 2103 K – ZnS) and can sublimate under high temperature with dissociation ($AB \rightarrow A + 1/2B_2$) [7, 12, 16-17]. At this temperature, the difference between values of pressure can reach several orders (Fig. 1).
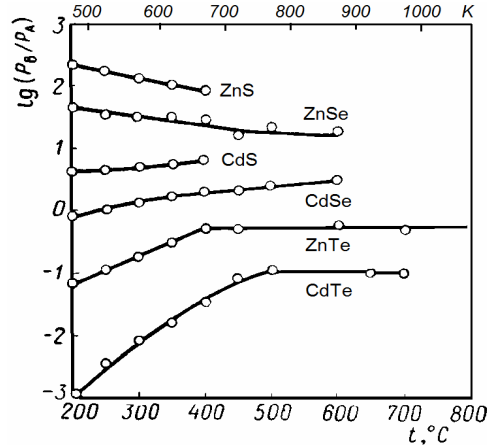

Fig. 1 − *Relation between equilibrium pressure of the cadmium and zinc chalcogenides components under different temperature of evaporation* [12]

This complicates the deposition of the stoichiometric films. According to Fig.1, the easiest to obtain stoichiometricaly are CdSe films and most difficult are ZnS and CdTe, due to the high rate of metal component desorption from the substrate [12]. Some properties of the cadmium and zinc chalcogenides are presented in Table 1.

Table 1 − *Some properties of the cadmium and zinc chalcogenides* [7, 10, 12, 16, 17]

Compounds	Melting point T_m, К	ZB a, nm	WZ a,c, nm	c/a	Stable phase	Density ρ 10³ kg·m⁻³	Coef. of expansion $\alpha \cdot 10^{-6}$, K⁻¹	Band-gap E_g, eV (300 K)	Conductivity
ZnS	2196 [17] 2038 [7] 2103 [12]	0.54093	0.3820 0.6260	1.639	ZB	4.090 (ZB)	6.14	3.68	*n*
ZnSe	1793 [17] 1797 [7] 1788 [12]	0.56687	0.4003 0.6540	1.634	ZB?	5.264 (ZB)	9.44	2.67	*n*
ZnTe	1568 [17] 1513 [7] 1568 [12]	0.61033	0.4310 0.7090	1.645	ZB	5.633 (ZB)	8.40	2.26	*p*
CdS	1748 [17] 1678 [12] 1748 [12]	0.5820	0.41368 0.67136	1.624	WZ	4.825 (WZ)	4.50	2.53	*n*
CdSe	1531 [17] 1623 [7] 1531 [12]	0.6051	0.4304 0.7018	1.631	WZ	5.655 (WZ)	6.26 4.28	1.70	*n*
CdTe	1365 [17] 1370 [7] 1371 [12]	0.6482	0.457 0.747	1.635	ZB	5.850 (ZB)	4.90	1.46	*p,n*

Under thermodynamically equilibrium conditions cadmium and zinc chalcogenides crystallize to cubic modification with sphalerite structure and hexagonal modification with wurtzite structure (Fig. 2). The cubic modification have T_d^2 (F4$_3$m) symmetry group and hexagonal modification have C_{6v}^4 (P6$_3$mc) symmetry group.
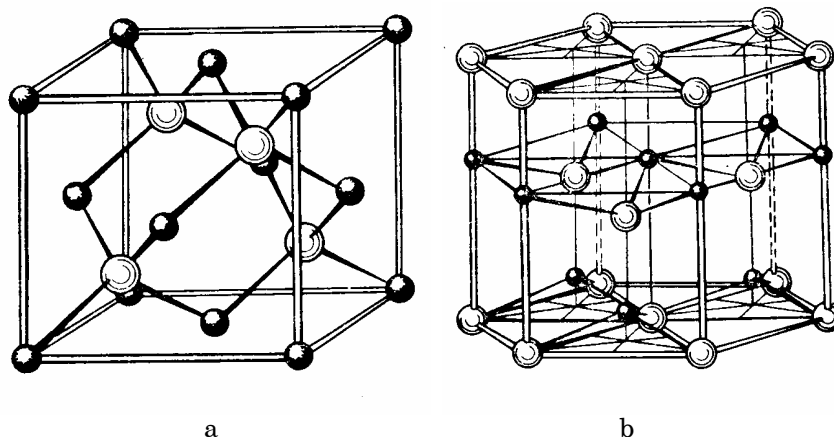

a   b

Fig. 2 – Unit cells of the cubic (sphalerite) (a) and hexagonal (wurtzite) phases (b) of thechalcogenides

In both crystal lattices every ions of II group elements is surrounded by the ions of VI group elements and conversely. In addition, these structures can be described as close packing of chalcogenide atoms and metals ions situated in tetragonal spaces. Sphalerite structure corresponds to cubic (3C) close packing ...AaBbCcAaBbCc...of the crystallographic planes, at the same time the wurtzite structure corresponds to hexagonal (2H) close packing ...AaBbAaBbAaBb.... These two can be differentiated only by the alternation of the crystallographic planes [12, 20].

Failures of the crystal lattice sequence can produce SFD, which can be described as faults in three-level cubic sequence and two-level hexagonal phase appearance (Fig. 3 a) [20-21]. The 2- and 3-type SFD are called deformation defects, and 1-type SFD are called twins. If the faults in crystal sequence are periodical then the polytypes along (0001) WZ or (111) ZB direction can appear. The SFD and polytypes always appear in single-crystal and thin films because the energy of SFD formation is rather low (Fig. 3 b). For example, in ZnS there exist more that 150 polytypes [21]. Often the zinc and cadmium chalcogenides layers are polymorphous and include both phases. Coexistence of two phases can be explained by the similar value of the energies of phase's creation, and low energy of interphase sphalerite-wurtzite (Table 2) [12].

The lattice parameters of the sphalerite and wurtzite can be expressed as $a_W = \sqrt{2}/2\,a_{ZB}$, $c_W = 2\sqrt{3}c_{ZB}$, respectively. The phase's stability depends on growth conditions of the single crystal or films, concentration of the impurity, deviation from the stoichiometry. The metal excess is stabilized hexagonal phase, whereas chalcogenide excess has cubic phase. Materials doping by the donor impurities (Al, In, Ga) lead to stabilization of the

hexagonal phase and doping by the acceptor impurities (Cu, Ag, Au) stabilizes sphalerite phase. Phase transition, which is activated by the impurities, depends on the formation of the local faults in the crystal lattice. For the compounds with coordination tetrahedron, the relation for the phase stability at normal conditions was determined empirically. For the crystal with lattice parameters ratio $c/a = 1.625$ the hexagonal phase is stable. In the range of $1.625 < c/a < 1.633$ the transition between sphalerite and wurtzite occurred relatively easily and depends on growth conditions, concentration of the impurity, and deviation from the stoichiometry.
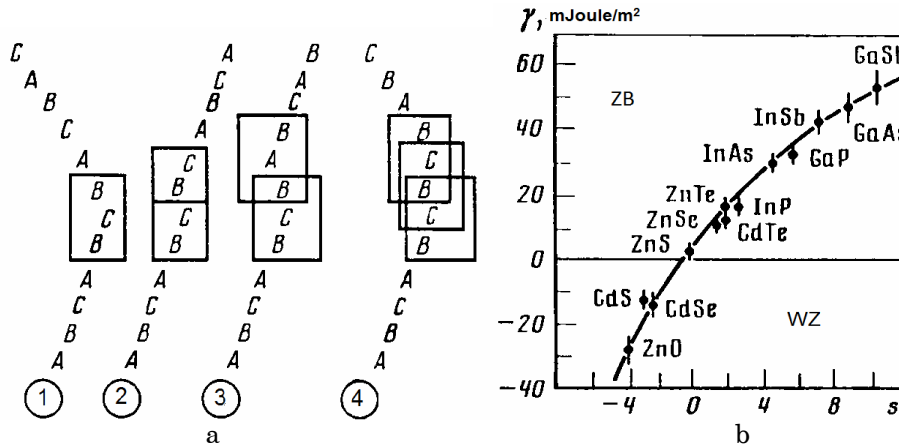

Fig. 3 − *Different types of SFD and energies of SFD formation in semiconductors at effective charge s* [21]

Table 2 − *Energies of sphalerite and wurtzite phase's creation* [12]

Compound	u_{0ZB}, eV/mol	u_{0WZ}, eV/mol	Δu, eV/mol
ZnS	35.787	35.787	0
ZnSe	34.443	34.387	+0.056
ZnTe	32.271	32.206	+0.065
CdS	33.455	33.494	-0.039
CdSe	32.375	32.328	+0.047
CdTe	30.529	-	-

For the crystal with $c/a > 1.633$, the cubic phase is stable [10]. The lattice parameters and lattice parameters ratios for the different compounds are presented in Table 1. As follows from Table 1, in thermodynamically equilibrium conditions ZnS, ZnSe, and ZnTe should have cubic structure, CdS − hexagonal, and CdSe a mixed structure. The probability of metastable phase formation is increased for samples obtained under far from equilibrium growth conditions.

2.2 The influence of point defects structure on optical and electrical properties of the films

The important factor that determines the structural properties of the II-VI compounds is the concentration of different types of the defects. The defects

can be separated as point defects, one-, two- and three-dimensional [20]. As a point defect the vacancies (VA, VB), interstitial atoms (Ai, Bi), antistructural defects (AB, BA), and impurities (CA, CB) at sites and interstitial impurities (Ci) are considered [5, 9, 20, 21]. However, for a wide-band gap semiconductor (except CdTe) the antistructural defects are not typical and appear only under ionizing radiation [22]. Point defects in II-VI compounds can be singly or doubly charged. Every native point defect generates a localized center in BG, of energy level, ΔE_i, which can be either near the valence or conduction band according to donor or acceptor defects, respectively, or near the mid-gap traps and recombination centers. The influence of point defects structure on the electrical properties of the semiconductor materials is considered in [5, 9, 21, 22]. It should be noted that in spite of plenty of research a unified model of the point defect creation in chalcogenides is not established yet [9, 21, 22]. The screw and edge dislocations, which can be situated in the crystallite volume or can be formed near low-angle grain boundary, are identified as another type of the defects. A third type of the defect includes SFD, twins, grain boundaries, and crystallite surfaces. The last type of the defects is related to creation of voids and inclusion of spurious [20].

According to the theoretical approaches developed by I.E. Tamms in finite semiconductor materials, it is possible for the formation of allowed energy states, which are unresolved in the infinite crystal lattice. Furthermore, experimental researches of high purity surfaces of the GaAs, InP, GaSb compound semiconductors have shown that the eigenstates are absent in such surfaces [13, 28].

Energy states near the surface can appear due to adsorption of gas atoms (first of all oxygen) and formation of different types of the defects. That assumption can be applied to grain boundaries, inclusions, and voids [13].

The system of the surface energy states lead to localization of the free charge carriers. This surface charge is neutralized by the space charge, as a result a double charge layer is formed (Fig. 4 a). In semiconductors, this layer can have thickness (Debye length) about one μm. It is related to bending of valence and conduction band edge near the grain boundary on the energy diagram [13, 30, 31].

The depletion, inversion, or enriched layers can be formed depending on the nature of the surface states and their energy distribution (Fig. 4 b). In most cases, the depletion layer is formed on the intrinsic materials' interfaces. The enriched layer is formed in doped materials. Thus, charge carrier trapping can lead to increasing (decreasing) the conductivity of the film [13, 30, 31].

It should be noted that the electrical activity of the different grain boundaries is different. The minimal activity have boundary between coherent twins and maximal large-angle boundaries. The last one has a high concentration of the dislocation, a high deformation of the crystal lattice and impurity segregation.
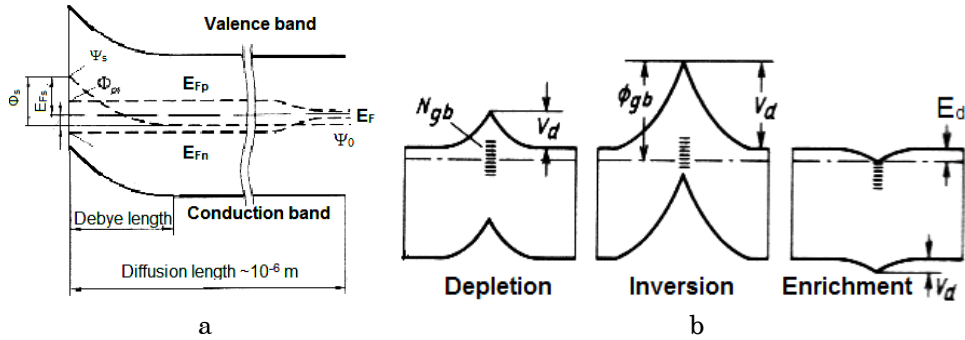
Fig. 4 − Energy band diagram near-surface region of the n-type semiconductor (a) and three cases of the possible potential barrier at the grain boundary (b). E_F − Fermi level; V_d − potential barrier height [13]

They are substantially determining the electrical properties of the polycrystalline material. The devices with separating barriers (photodetectors, solar cells, etc.) classify according to the influence of grain boundary on the device's performance into two types, namely: with parallel and perpendicular barrier. The light generated charge carriers beyond parallel p-n junction or heterojunction almost completely recombine at the grain boundary states and do not contribute to the photocurrent and, in addition, the mobility of the charge carriers in polycrystalline films is considerably less than in single-crystal, which decreases the device's performance [13, 30, 31]. Petritz [32] and Seto [33] obtained the expression for charge carrier's mobility in polycrystalline films. Grain boundaries which are parallel to the separating barriers lead to decreasing of the short-circuit current I_{sc} and the open-circuit voltage U_{oc}, and increasing of the loss current of the solar cells. For minimizing the loss the grain of the polycrystalline films should be columnar-like with its size more than double the diffusion length ($d >> 2L_{dif}$). A more detail discussion of the influence of grain boundary on device's performance is described in [13, 30-33]. Energy diagram of the II-VI layers that contain dislocations also have a number of peculiarities. For instance, near the edge dislocation there exist regions of compression and stretching, which leads to a local change of the energy band gap due to the variation of the interatomic distance (Fig. 5) [5-6]. This leads to an absorption of the photon with $h\nu < E_g$ energy, that is equal to formation in BG dislocation levels, which can split and form energy band. Existence of such dislocation levels can be detected by the low-temperature photoluminescence (Y-band) in deformed compound crystal. Thus, the transition between dislocation levels and allowed bands are possible. The light absorption on these transitions will be weak due to the low density of dislocation-localized states. However, these states can decrease free carrier lifetime and hence increase (or decrease) the film's conductivity.

In addition, in II-VI compounds there exist high fields near the dislocation, which can cause affect the slope of the band edges and stimulate interband transitions according to Franz-Keldysh mechanism (Fig. 6). It was determined that the influence of this effect on the absorption spectrum edge is more substantial than the influence of the deformation potential [5-6].
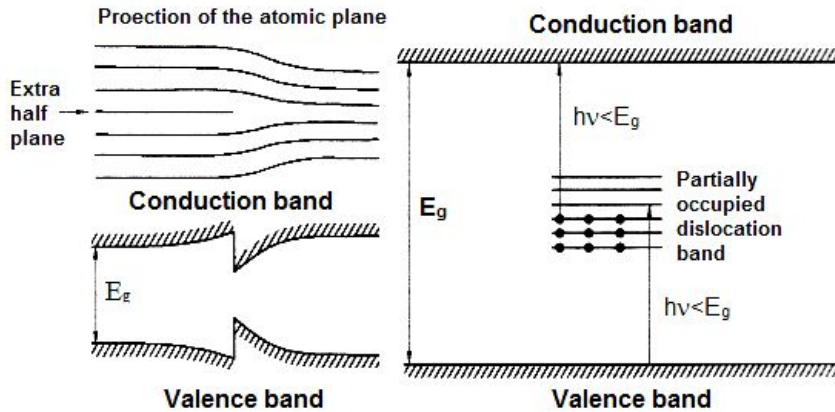
Fig. 5 − *Local change of the BG near the edge of the dislocation and corresponding energy diagram* [5-6]

Substantial bending of the energy band can lead to discharge or filling of the point defects localized states near the dislocation. In turn, it leads to optical transitions that can be observed in dislocation-free material.
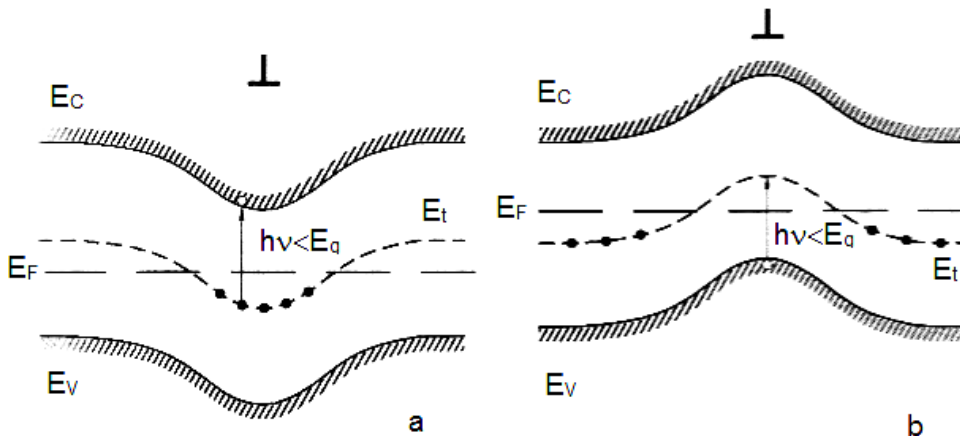

Fig. 6 − *Bending of the energy band near the positive (a) and negative (b) charged dislocation. E_t − point defects levels, E_F − Fermi energy*

Deviations from the stoichiometry outside the homogeneity region lead to the formation of precipitates. As a rule, precipitates are formed near the structural defects (first of all grain boundaries) and can shunt it [12-13]. Such native point defects have influence on the electrical properties of II-VI single crystal.

2.3 Chalcogenide thin films deposition methods

Nowadays, for the cadmium and tellurium chalcogenide thin films different deposition methods are used, among them: chemical spray pyrolysis [34], high-frequency magnetron and reactive sputtering [35-36], deposition from water solution [37-39], electrochemical deposition [40-42], electron-beam

[43], laser-pulsed [44], thermal evaporation of the compound [24, 25, 45-47] or compound components [48], hot-wall evaporation (close-spaced sublimation) [49], molecular-beam epitaxy [50-51], metal-organic vapour deposition [52] and others. Every method mentioned above has its advantages and disadvantages.

Depending on the type of substrate, the polycrystalline or epitaxial films can be obtained by different methods [34-52]. The II- VI epitaxial films can be obtained on Ge, Si and III-VI single crystal (Fig. 7) [4] substrate matched to films material for lattice parameters and thermal expansion coefficient by the methods that provides close to equilibrium growth conditions: molecular beam epitaxial, metal-organic vapour deposition or close-spaced sublimation (CSS). The glass, tin, zinc, steel oxide non-oriented substrates are usually used for polycrystalline film deposition.

The undoped II-VI films were obtained in Refs [26-28, 36-46, 49-52], at the same time in Refs [12, 35, 47, 48] the doped ones with differing impurities were deposited. In most works, the elements of I, III, V, and VII group were used.

Among the different thin film deposition methods the vacuum deposition of the films can be considered as the most promising due to versatility and possibility of condensation of the high-purity layers. As a rule, a few types of this method are used, which are differentiated by the evaporation methods (thermal, electron-beam, laser, etc.) and charge composition that is evaporated (compounds or chemical elements).
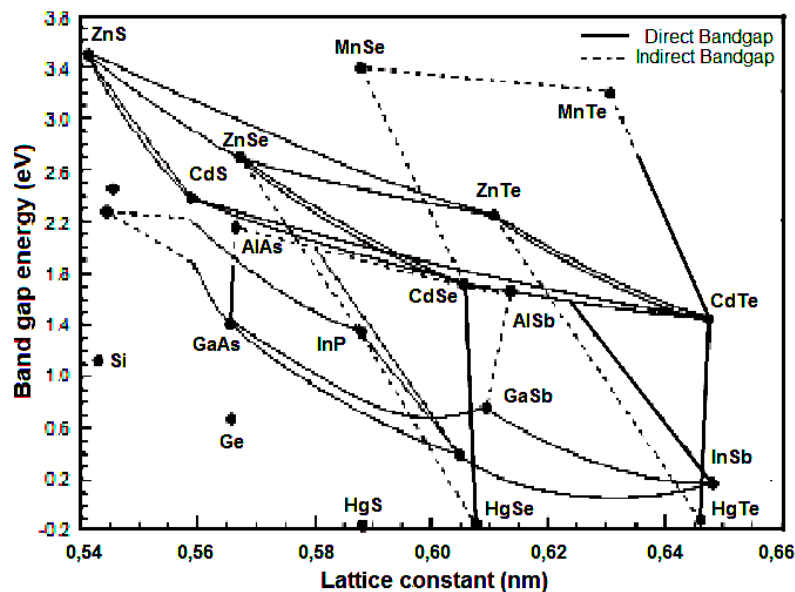

Fig. 7 − *Dependence of band-gap energy on lattice parameter of the* [4]

Let us consider the CSS method in more detail. Owing to technical features of the evaporator, the CSS method allows to grow high-quality semiconductor thin films under controllable technological process [13, 49]. It should be noted that the CSS method allows one to obtain thin films under

close to thermodynamically equilibrium growth conditions at high substrate temperature T_s and a small difference between substrate temperature and evaporation temperature ΔT ($\Delta T = T_e - T_s$). The design of the CSS methods equipment is described in [13]. However, influence of growth conditions on structural and substructural properties of zinc and cadmium chalcogenides thin films obtained on non-oriented substrate is not studied well. Corresponding researches have been executed in [53-74]. For example in [64] the structural properties of the ZnSe films obtained at room temperature was carried out, a more detail study of the films deposited at substrate temperature (473-623) K was performed in [63]. Some structural and optical properties of CdSe films obtained at a rather narrow substrate temperature range (290-490) K were studied in [70]. The structural, optical, and electrical properties of the ZnTe films obtained at $T_s = (293\text{-}450)$ K ($T_e = (1000\text{-}1250)$ K) on a glass substrate have been studied in [68]. The polycrystalline ZnTe thin films had cubic structure, but in [67] the hexagonal phase in ZnTe was detected. The deterioration of the (111) texture after annealing at $T = 475$ K was observed. The lattice parameter, scattering domain size (SDS), and the surface roughness was also determined in [68]. Further studies have been done to elucidate the structural, electrical, and optical properties of Zn doped CdTe films [69]. The $Cd_{1-x}Zn_xTe$ ($x = 0.4$) thin films obtained by the CSS method was studied in [75]. Some of above-mentioned results are presented in Table 3.

Table 3 – *Structural properties of the ZnTe films obtained by the thermal evaporation*

T_s, K	d, μm	(hkl)	2θ, Degres	d_{hkl}, nm	a, nm	L, nm	$\sigma 10^{-9}$, Pa	$\rho \cdot 10^{15}$, lin/m^2	Reference
ZnSe									
300	0.13	(111)	31.7	0.328	0.5672	19.24	-	-	[64]
	0,30	(111)	31.7	0.328	0.5672	16.74	-	-	
	0.85	(111)	31.7	0.328	0.5672	45,24	-	-	
473-623	0,25	(111)	27.24		0.566-0,571	10-48	− 0.2-0.8	1-35	[63]
ZnTe									
293	0.24	(111)	29.2	0.354	0.6089	57.3	-	-	[68]
		(222)	60.8	0.177	0.6110	24.4	-	-	
450	2.53	(111)	29.2	0.354	0.6089	42.2	-	-	
		(220)	48.9	0.216	0.6109	41.6	-	-	
		(311)	58.2	0.184	0.6102	25.8	-	-	
		(222)	60.9	0.177	0.6110	32.3	-	-	

It should be noted that the calculation of the lattice parameter and substructural properties of the zinc and cadmium chalcogenides thin films was carried out for the (111) planes at small angles. It leads to significant error in the value of lattice parameter. Only in [68] the Nelson-Relay method was used which provides results that are more precise. Although the Debye-Scherrer equation was applied for determining SDS, this equation does not take into account microdeformation and SFD in thin films.

2.4 Structural properties of the chalcogenide thin films obtained by the CSS method

It is well known that growth conditions have a strong effect on structural, electrical, and optical properties of the II-VI thin films. The substrate T_s and evaporator T_e temperatures are the main parameters for CSS deposition [13, 49]. Some structural peculiarities of the II-VI films (CdSe and CdTe) obtained by the CSS on the mica single-crystal substrates have been studied in [13]. In this work, the influence of growth conditions on structural and substructural properties of the films obtained by the CSS is based on the results of previous studies [75-88]. The glass, glass-ceramic or metallized (Mo for CdTe, CdSe and ZnS, Cr for ZnTe) glass-ceramic substrates are used as substrates for zinc and cadmium chalcogenides deposition. It was determined that films deposited on non-oriented substrate at $T_s > 373$ K have homogenous surface and good adhesion to substrate.

The growth mechanism of compounds with sphalerite structure was the same. The fine-crystalline layer ((0.01-0.05) μm crystallites size) near substrate is condensated in the first place, after that the crystallites overgrow parallel to the (111) plane without coalescence.

In case of thin films with wurtzite structure the crystallites growth occurred parallel to the substrate and was oriented by the (002) plane. Because of the X-ray diffraction and scanning electron analysis [75, 77, 83-87] it was determined that the two different growth conditions of zinc and cadmium chalcogenide films correspond to the same growth mechanism. At low substrate temperature, less by a third than the melting point, the crystallites overgrowth did not occur due to secondary nucleation on the grain surface.

The crystallites have equiaxial, close to spherical shape (Fig. 8 a) and size of about (0.1-0.5) μm, and crystallites size increasing with T_s (Fig 9, 10). At a high substrate temperature, more by a third than the melting point, the growth mechanism is changed. It led to formation of the big columnar grain (Fig. 8) oriented in the (111) plane. As a result the grains have axial growth texture (111) orthogonal to the films surface. The CdTe films have most and ZnS least pronounced columnar growth mechanism. Corresponding II-VI films cross sections are presented on Fig. 8.

For the columnar defects in the thin films, the substantial overgrowth of the grains is typical, and this process is more intensive at a "small" d value. The size of the crystallites depend on the film's thickness and growth conditions; at a critical thickness d_{cr} the increasing of the grain size is decelerated due to secondary nucleation and blocking of closely spaced grain. At close to equilibrium growth conditions and ΔT about (30-100) K, the films with pronounced columnar growth structure are formed. The diameter of the columnar grains depends on growth conditions and the film's thickness (Fig. 9). The average grain size increases with ΔT decreasing, and also depends on the type of material. The biggest average grain size occurs in CdTe films, the smaller in CdSe, ZnTe (Fig. 10), and the smallest in ZnS (Fig.9); this corresponds to different melting points of these compounds.

The increasing of the grain size is accentuated with substrate temperature more than critical values and small ΔT, which can be explained by the change of the gas transport regime between evaporator and substrate

from molecular to gas-dynamic and rapid decreasing of vapor supersaturation at high substrate temperature. At higher substrate temperature, the etching of film occurs, and on further increase in temperature, the island kind of growth was obtained.

Increasing of grain sizes lead to formation of strong surface binding and increasing of surface roughness R_a (for CdTe R_a = (0.64-1.34) μm, for ZnTe R_a = (0.93-1.41) μm) for substrate temperature T_s changing from 423 to 823 K [79, 81].

It is well-known that II-VI layers are polymorphic and often consist of cubic and hexagonal phase. During the storage or thermal processing of the film, a change in its phase composition leads to fluctuation of the electrical and optical properties of the films. Therefore, for the device manufacture only films with stable structure are used. This explains the importance of phase analysis of layers. Corresponding studies for chalcoge-nide films obtained by the CSS was carried out in [75-77, 83, 85, 88]. The X-ray diffraction patterns of the zinc and cadmium chalcogenide films are presented in Figs. 11, 12.

From Fig. 11 we see that only the reflections from (111), (220), (311), (222), (331), (422) planes of the cubic phase are observed on the patterns of the ZnTe and CdTe films obtained at high substrate temperature and ZnS, ZnSe films obtained at low substrate temperature. The most insensitive in most cases was the (111) peak, which corresponds to high growth (111) texture in cubic films.
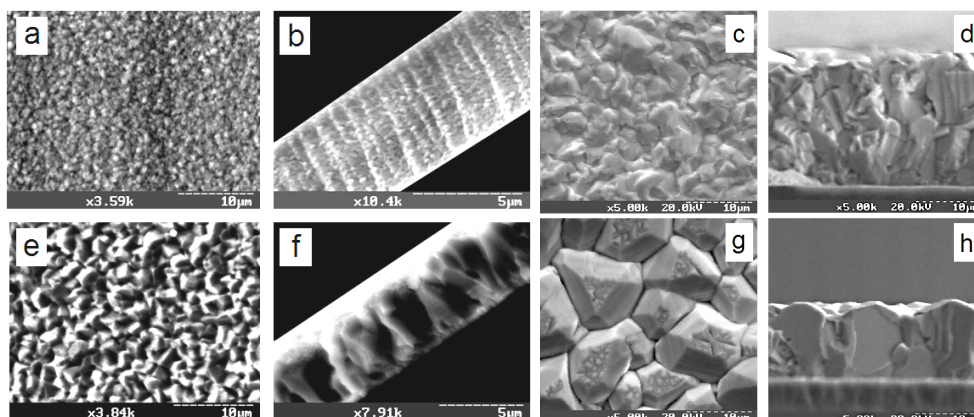

Fig. 8 − *SEM images of the CdSe films, obtained at different growth conditions: T_e = 893 K: T_s = 473 K (a, b); T_s = 873 K (e, f); and CdTe: T_e = 893 K: T_s = 698 K (c, d); T_s = 798 K (g, h) and films cross-sections (b, f, d, h)*

The X-ray analysis of ZnTe films, obtained at different growth conditions, show that they have a cubic structure, but the hexagonal phase was not recognized (Fig. 11 b) [75].

X-ray patterns of the CdTe films obtained at T_s < (473-523) K usually show the peaks from planes of the stable cubic phase and peak from (101) plane at 2θ = (24.8-25.2)° with intensity less than 1 % was observed. This peak corresponds to the trace (2-3 % concentration) of the metastable wurtzite

phase. Sometimes the reflection from hexagonal phase with less intensity at $22.2°$ -$22.3°$ − (100) and at $42.8°$-$42.9°$ − (103) was detected (Fig. 12).

It should be noted that the concentration of hexagonal phase increases with a decrease in the film's thickness, which can be explained by the formation of the metastable phase in the transmission layer near the substrate. The CdTe films obtained at $T_s > 523$ K corresponds to a single cubic phase only [85].
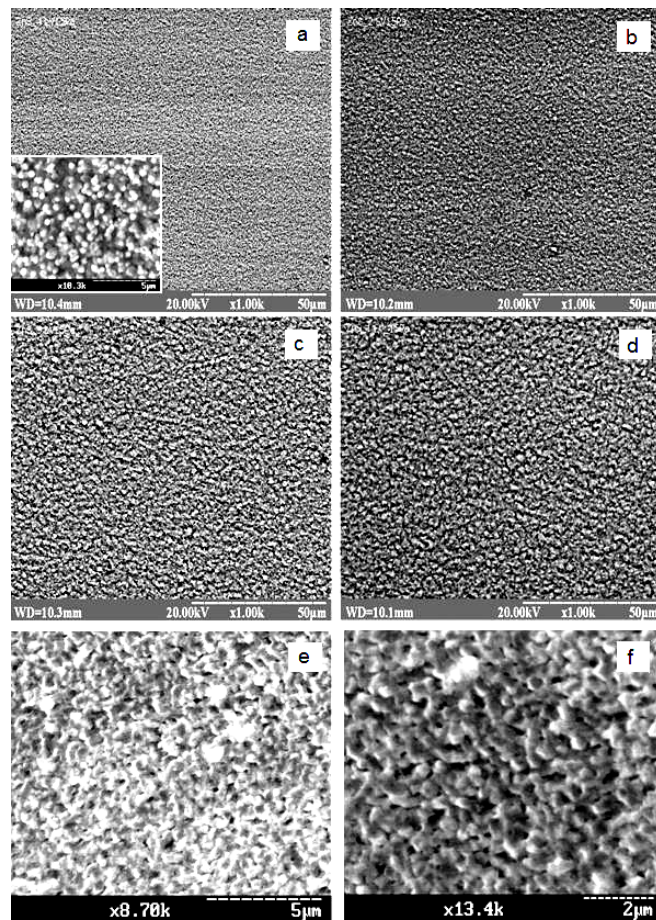

Fig. 9 *– SEM images of the ZnS films ($d \sim 10$ μm; $T_e = 1173$ K), obtained at different T_s: 473 K (a); 573 K (b); 773 K (c); 973 K (d); 473 K (×8700) (e); 473 K (× 13400) (f)*

The analysis of X-ray diffraction patterns demonstrated that ZnS films grown at $373 < T_s < 573$ K have cubic crystalline structure. Hexagonal phase in condensates was not observed in X-ray diffractograms (Fig. 11). At $T_s > 573$ K the traces of hexagonal phase are appearing in ZnS films, their amount somewhat increases under increasing the substrate temperature. So, the zinc sulfide films obtained at high substrate temperature are double-phased compounds [80, 83]. A similar result was obtained for the ZnSe thin films;
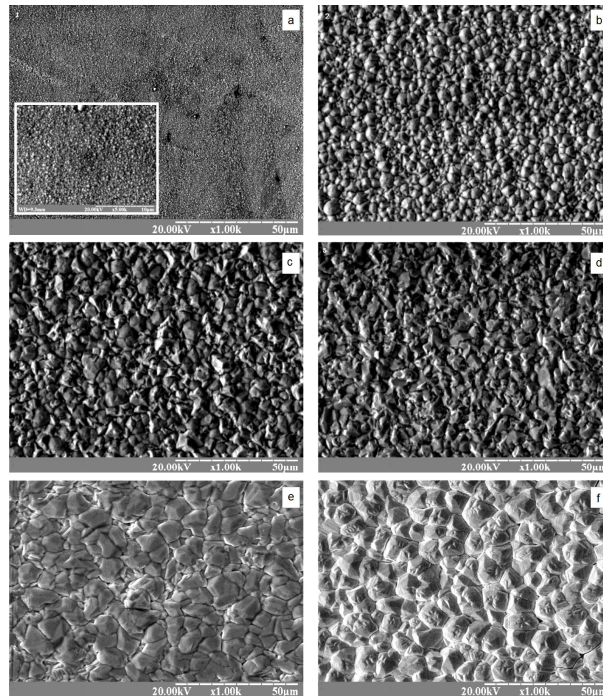
Fig. 10 *− SEM images of the ZnTe (d ~ 10 μm, T_e = 973 K), obtained at different T_s: 473 K (a); 573 K (b); 673 K (c); 773 K (d), 823 K (e), 873 K (f)*

however, the concentration of the hexagonal phase was less than in ZnS films, and did not exceed a few percent [87]. The X-ray diffraction patterns of the CdSe films obtained at different substrate temperatures are presented in Fig. 12 (d, f). The X-ray patterns show the reflection from (100), (002), (101), (110), (103), (112), (203) planes.

The most intensive peaks were (002) and (102), which corresponds to growth texture orthogonal to these planes. However, in CdSe films obtained at T_s = (373-473) K an additional peak is observed at $2\theta \sim 60.90°$ that can be considered as reflection from the (400) planes of the cubic phase. The lattice parameter calculated by this peak was a = (0.6075-0.6080) nm, this value is in good agreement with reference data a = 0.6077 nm [89]. It allows us to surmise that the films obtained at low substrate temperature have two-phase structure. For the CdSe films obtained at high substrate temperature (T_s > 473 K) only wurtzite phase was observed [88].

The obtained results are in good agreement with the calculations of the polymorph phase's formation in II-VI compound [12] according to which the stability of zinc blend structure increases in compounds ranging from CdS-ZnS-CdSe-ZnSe-CdTe-ZnTe. That is why in ZnTe films the formation of the hexagonal phase is improbable (Δu_{ZB-WZ} = 0.065 eV/mol). In CdTe films obtained at low temperature and ZnSe films obtained at high temperature (Δu_{ZB-WZ} = 0.056 eV/mol) this phase exist in the transmission layer near the substrate. The CdSe has hexagonal phase for the whole substrate temperature range. Only ZnS films have a cubic structure; however, the
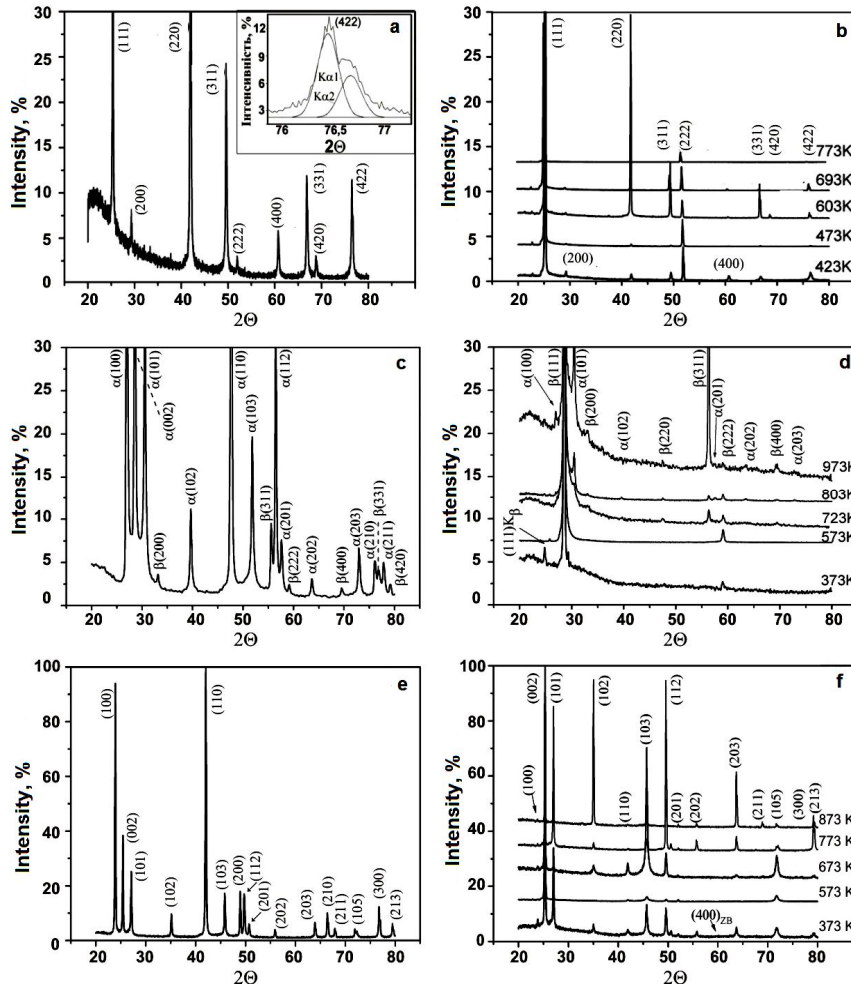
Fig. 11 − *X-ray diffraction patterns of the charge (a, c, e) and ZnTe (b), ZnS (d) and CdSe (f) films obtained at different T_s*
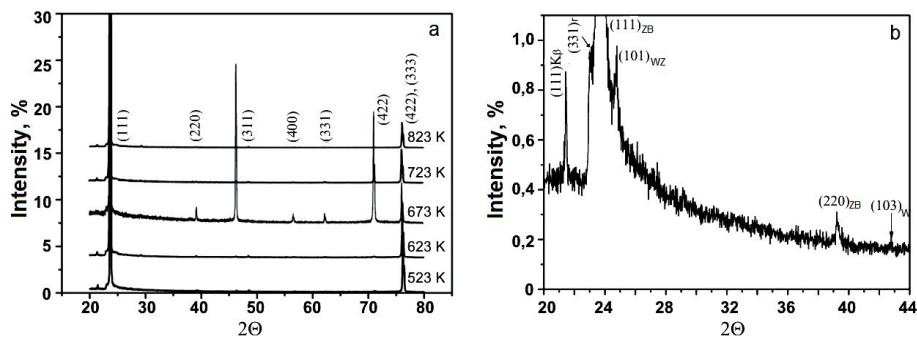

Fig. 12 − *X-ray diffraction patterns of the CdTe films, obtained at different T_s (a) and range of pattern of the film obtained at $T_s = 523$ K (b)*

hexagonal phase was detected in layers obtained at high substrate temperature ($\Delta u_{ZB\text{-}WZ} = 0$).

As it was shown by the high-resolution electron microscopy studies performed for CdTe films [90] the hexagonal phase in A_2B_6 compound is formed due to distortion of alternating order of close-packed planes, but not as separate grains: the transition from trilayer packing ...AaBbCcAaBbCc... typical for the zincblende structure to the bilayered ...AaBbAaBbAaBb... packing calls for the formation of WZ structure. As a result the cubic matrix with a large amount of SFD and an interlayers of the hexagonal phase appears, and this matrix is conjugated $((110)_{ZB} \parallel (110)_{WZ}$, $(111)_{ZB} \parallel (001)_{WZ})$ with the ZB structure. This fact creates difficulties for revelation of the WZ-phase by the X-ray methods [14-15], thus concentration of metastable phase detected in [80, 83, 87, 88] can be underestimated.

Calculations by the reciprocal pole figures method [91-94] allowed determining the axial growth texture (111) in chalcogenide thin films, which is increased with layers thickness and depends on growth conditions (Fig. 13) [80, 83, 85, 87]. In CdSe layers with hexagonal structure obtained at $T_s \leq 773$ K, calculations of pole density $P_{(hkl)}$ allows to determine the axial growth texture (002). The texture perfection depends on the growth conditions and the film's thickness. In films obtained at $T_s \geq 773$ K this texture is changed to (102) [88].

The growth texture (110), (112), (102) in CdSe thin films obtained by the thermal evaporation was observed in [45], also. From the dependence of the orientation factor on substrate temperature, as seen from Fig. 14, the thin films were high-textured at rather high and low substrate temperatures. In films obtained at intermediate temperatures texture was less pronounced. At these temperatures, the concentration of the crystallites with different orientations in films was increased. This can lead to a change of the growth texture. It was determined that the temperature that corresponds to a decrease of the texture quality depends on the type of the compound.
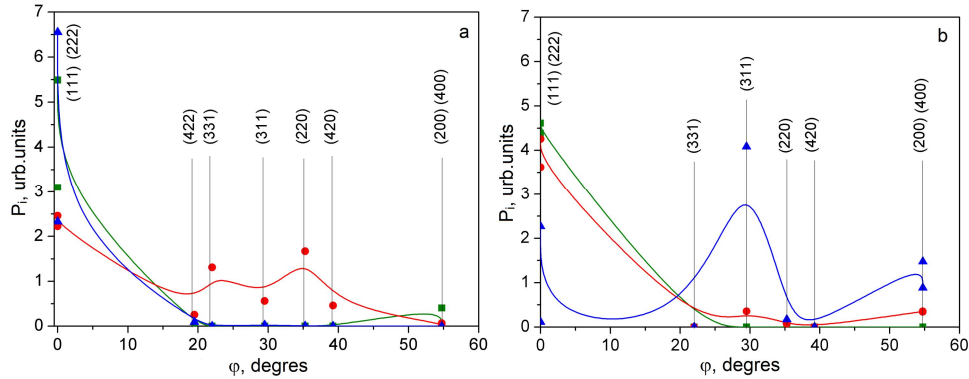

Fig. 13 − *The pole density P_i at φ angle between texture axis and normal to reflection plane for the ZnTe ($T_s = 323$ K (■), 603 K (●), 773 K (▲)) and ZnS ($T_s = 373$ K (■), 723 K (●), 973 K (▲))*
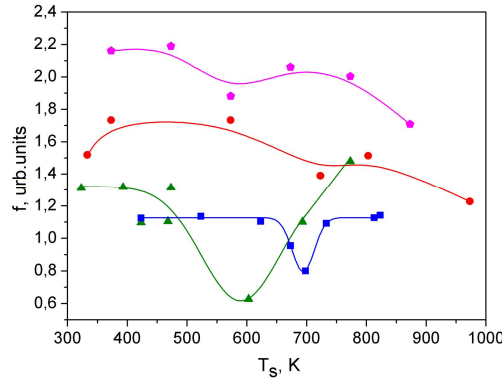
Fig. 14 − *Dependencies of the orientation factor f at substrate temperature T_s for the ZnTe (▲), ZnS (●), CdTe (■) films with cubic structure and hexagonal CdSe films (⬟)*

The decreasing of the films texture at intermediate temperatures, except [80, 83, 85, 87], was observed in [61] for CdTe films. However a minimum on f-T_s dependencies was observed in other temperature range (T_s = (600-625) K). A decrease in the texture of the chalcogenide layers can be caused by the changing of the growth mechanism from layer-to-layer to columnar-like. In addition, it was determined that the (111) texture in cubic and (002) hexagonal layers decreased at close to equilibrium growth conditions when the optimal energy for the crystallites' growth is oriented parallel to the substrate.

2.5 Substructural peculiarities of chalcogenide thin films

Substructure peculiarities of chalcogenide thin films deposited by CSVS method are not practically investigated. At the same time, dislocations, which constitute low-angled SDS size boundaries and give rise to microdeformation in films, that may be used as traps and deep recombination centers, which determine the electrical characteristics of chalcogenides films.

X-ray analysis was used to determine the SDS size, microdeformation level, and concentrations of other structure defects of chalcogenide films in Refs. [78, 81, 83, 85-87]. It is well-known [91-94] that the widening of the X-ray lines, apart from instrumental effects, it endorses deposit of small SDS sizes (*L*), microdeformations ($\varepsilon = \Delta d/d$), and SFD. Recent methods of analysis X-ray lines' widening, determining L and ε, are well-developed and widely used in investigation of polycrystalline metal films, plastic deformations, disintegration processes of oversaturated solid solutions, local, structural, and chemical metal transformations. For investigation of metal semiconductor chalcogenides films, such methods were rarely used. Usually in well-known researches [53, 54, 55, 56, 63, 64, 68, 72], it is considered that the widening of diffraction peak is due mainly to SDS size dispersion whereas the presence of microdeformations and SFD contributions are slight. To determine the blocks sizes one uses the Scherer equation $L = k\lambda/\beta cos\theta$, where $k \sim 0.9$ is a coefficient that weakly depends on the blocks' form. Microdeformation level is evaluated by change of the material lattice parameter of charge and film (see [53, 54, 55, 56, 63]). However, it

is not correct since as shown in works [75, 79, 83, 85], the lattice parameter of chalcogenide compounds diverges from their stoichiometric composition. The study of the substructural characteristics of vacuum chalcogenide condensates with cubic structure was estimated by the widening of diffraction peaks (111)-(222) and (200)-(400) of this phase in Refs. [78, 81-83, 85, 87]. Unfortunately, in some cases reflections from ares/planes (200), (400) were not fixed because of the films grain-oriented, therefore some information about substructural peculiarities of films was lost. Substructural parameters of films with hexagonal structure was estimated by a physical widening of diffraction peaks (100)-(200), (101)-(202) and (002)-(105) [86]. A treatment of the experimental results in most cases was to consider that mechanical characteristics of films are isotropic. For examination of obtained L and ε values precision at this approach in line of cases allows for microstresses anisotropy in condensates. In work [78] it has been done for ZnTe.

Typical Hall graphs for ZnTe films, which have a sphalerite structure, were obtained from analysis of X-ray lines half-width with and without consideration of the microstress anisotropy is presented in Fig. 15.

As analysis show the slopes of lines for (200) and (400) dots obtained with consideration of microstress anisotropy was lesser than without its consideration, but the lines crossed the y-axis practically at one point. Since the slope estimates the microdeformation level in films and the intercept on the y-axis gives SDS size in the direction perpendicular to the corresponding plane, we see that the microstress anisotropy brings only a change of values of the order of ε_{isotr} / $\varepsilon_{anisotr}$ = 1.5.

As shown in Fig. 15 dot belt by reflections from planes (hhh) and (h00), with consideration of microstress anisotropy, lie on two lines which have different slopes. It may be caused by a presence of SFD in films [96, 97].

Fig. 15 − *Hall Graphs belt on X-ray graph from ZnTe film deposited at T_s = 693 K, Gauss (a) and Cauchy (b) approximations. Without microstress anisotropy considering (○); with its considering (■)*

The L and ε values obtained using the approximated X-ray peaks forms by Cauchy and Gauss [91-94] functions for cubic materials with consideration of the microstrain anisotropy are presented in Table 4.

From Table 4 the values of films' substructure parameters obtained, using two approximations, allows one to estimate only the most large and

most small values of SDS sizes L and microdeformations ε in films, with an experimental error of (30-50) % [91-95].

More precise determination of SDS sizes and microdeformation levels than the classical Hall approximation method uses the method based on three-fold functions convolution of X-ray line. The principles of estimating the films substructure parameters are expounded in [83, 97, 98].

The results of L and ε measurements using the three-fold convolution method are presented in Table 4, some of them are in Fig. 16. From Table 4 we see that the SDS sizes and microdeformation values obtained by three-fold convolution in most cases are intermediate between values obtained using Cauchy and Gauss approximations, according to theoretic point of view. It shows about the reliability of results presented in [78, 81, 83, 85]. In compliance with [97], SDS sizes and microdeformation level determination is precise for condensates by the three-fold convolution method and is no worse than (11-16) % depending on X-ray diffractogram survey conditions.

The dependence of SDS sizes and microdeformation levels in direction perpendicular to the atomic planes (111) and (200) for a given substrate temperature for ZnS films is presented in Fig. 16.

Table 4 − *Substructure characteristics of CdTe, ZnS and ZnTe sphalerite films obtained using different approximations*

T_s, К	(*hkl*)	L, nm			$\varepsilon 10^3$			α %
		Approximation by		From convolution	Approximation by		From convolution	
		Gauss	Cauchi		Gauss	Cauchi		
CdTe								
423	(111)-(222)	60.6	64.5	61.0	1.11	1.22	1.07	
	(200)-(400)							
523	(111)-(222)	64.5	74.5	64.9	0.94	0.74	0.64	
	(200)-(400)							
623	(111)-(222)	85.7	99.1	86.7	0.88	0.23	0.65	0.19
	(200)-(400)	100.7	110.8	101.2	0.47	0.17	0.31	
698	(111)-(222)	74.8	86.6	75.3	0.87	0.30	0.71	
	(200)-(400)							
733	(111)-(222)	72.3	81.5	72.9	0.93	0.22	0.68	
	(200)-(400)							
813	(111)-(222)	65.2	54.6	66.2	1.11	1.02	0.71	
	(200)-(400)							
823	(111)-(222)	56.6	51.2	56.9	1.02	0.75	0.69	0.79
	(200)-(400)	94.1	91.0	94.2	0.40	0.34	0.33	
ZnS								
Charge	(111)-(222)	46.7	36.5	59.0	0.26	0.66	1.24	1.22
	(200)-(400)	106.8	130.2	139.9	0.97	1.12	0.99	
373	(111)-(222)	30.9	36.2	37.1	1.65	1.87	1.05	-
	(200)-(400)	-	-	-	-	-		
473	(111)-(222)	46.1	39.8	39.5	0.36	0.48	0.32	-
	(200)-(400)	-	-	-	-	-		

T_s, К	(*hkl*)	L, nm			$\varepsilon 10^3$			$\alpha\%$
		Approximation by		From convolution	Approximation by		From convolution	
		Gauss	Cauchi		Gauss	Cauchi		
573	(111)-(222)	63.9	48.5	54.0	2.59	3.13	2.72	-
	(200)-(400)	-	-	-	-	-		
723	(111)-(222)	62.8	43.4	46.0	2.05	2.72	2.27	0.02
	(200)-(400)	63.9	47.1	46.3	2.33	1.96	2.46	
803	(111)-(222)	52.0	37.8	39.4	1.93	2.72	2.21	0.38
	(200)-(400)	57.1	48.2	46.7	1.46	2.34	1.84	
973	(111)-(222)	35.4	33.8	33.4	0.48	1.25	0.83	1.51
	(200)-(400)	74.1	71.4	70.7	0.51	0.76	0.45	
ZnTe								
Charge	(111)-(222)	28.6	36.5	37.5	2.03	2.05	1.19	1.43
	(200)-(400)	96.2	72.2	75.2	0.67	1.33	1.07	
323	(111)-(222)	46.6	58.0	59.4	0.87	1.60	1.29	0.67
	(200)-(400)	90.5	94.2	94.3	0.35	0.40	0.33	
423	(111)-(222)	64.8	63.9	63.9	0.70	1.37	1.11	0.53
	(200)-(400)	47.5	48.6	48.7	0.37	0.54	0.42	
468	(111)-(222)	69.4	65.4	65.5	0.15	0.63	0.43	0.12
	(200)-(400)	91.2	63.0	70.7	0.78	1.46	0.79	
473	(111)-(222)	54.2	60.4	60.8	0.72	0.93	0.64	-
	(200)-(400)	-	-	-	-	-	-	
603	(111)-(222)	65.4	68.8	68.9	0.45	0.62	0.46	0.15
	(200)-(400)	65.7	75.3	76.0	0.67	0.73	0.51	
693	(111)-(222)	74.5	67.1	67.5	0.17	0.88	0.64	0.04
	(200)-(400)	75.6	69.1	69.3	0.05	0.66	0.46	
773	(111)-(222)	59.1	62.0	62.1	0.46	0.66	0.49	-
	(200)-(400)	-	-	-	-	-	-	

Since the values of the parameters for the substructure of chalcogenides films obtained by three-fold convolution method are more precise, we shall discuss these results later on.

From Fig. 16 one can see that as T_s increases the size of SDS in the direction perpendicular to the planes (111) in ZnS films at first increases from $L \sim 37$ nm to $L \sim 54$ nm, later it decreases to $L \sim 33$ nm. In the temperature range $(T_s = (550\text{-}650) \text{ K})$ L is maximul. An increase of the substrate temperature leads to an increase of crystalline size in the direction (200). In authors [83] opinion the SDS size in the direction (111) is limited by the presence of SFD.
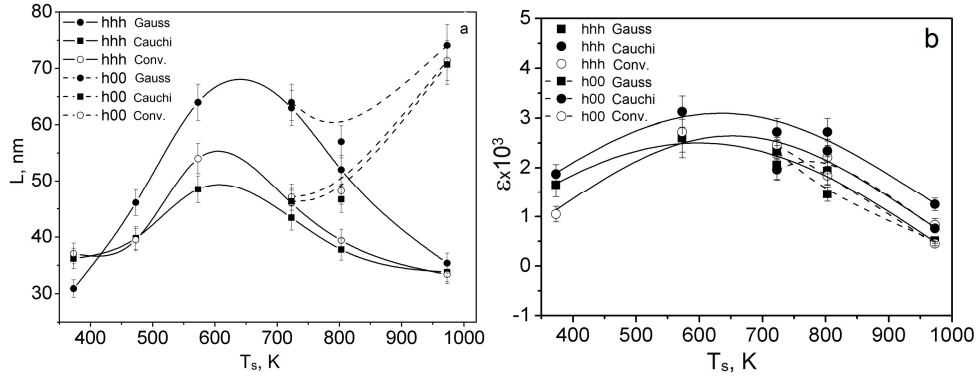
Fig. 16 − *Influence of surface temperature T_s on SDS size L (a) and microdeformation level ε (b) in ZnS films, measure was determined used three different approximations*

Microdeformation level of films in the direction (111) at first is increasing (from $\varepsilon = 1.05 \cdot 10^{-3}$ to $\varepsilon = 2.72 \cdot 10^{-3}$) and furthermore essentially decreases (to $\varepsilon \sim 0.83 \cdot 10^{-3}$) (Fig. 16 b). It should be noted that because of weak peaks, (200) and (400), the intensity measure of their half-width was determined by significant mistake so L and ε values in the direction (200) are less reliable than in the direction (111) [83].

Such peculiarities in the dependence of L-T_s were characteristic for another chalcogenides compounds with cubic phase. However, the material (Fig. 17 a, b) measured the average SDS size and temperature, which correspond to the maximal L value.

The determination of the average SDS size L and microdeformation level ε in CdSe films with hexagonal structure was estimated by the physical widening of diffraction peaks (100)-(200) and (002)-(105) [86, 88]. It may be left to determine in future the SDS size in the direction parallel (by widening of (002)-(105) lines) and perpendicular (by (100)-(200) lines) of c-axis for the crystalline wurtzite lattice. Since the hexagonal phase is so elaborate to determine, a reflection from the line of planes parallel to each other got out of planes and disorientated for small angles (210 for (002)-(105)). The results of the investigations are presented in Fig. 18.
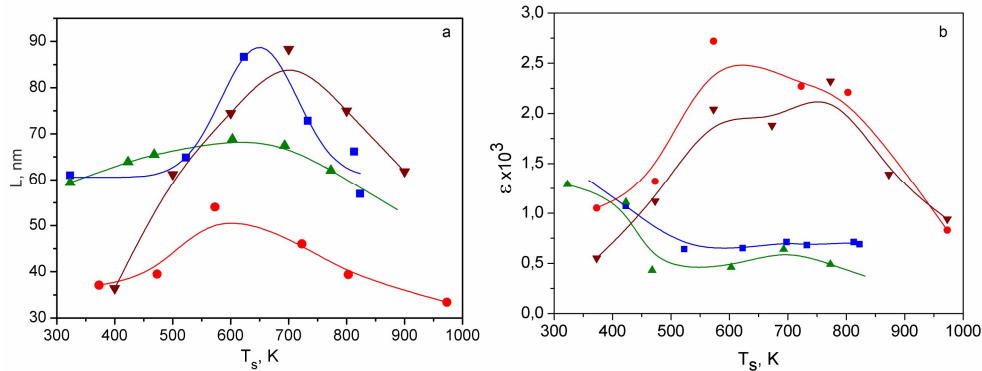

Fig. 17 − *Influence of substrate temperature T_s on SDS size L (a) and microdeformation level ε (β) of ZnTe films (▲), ZnS (●), ZnSe (▼), CdTe (■). Three-fold convolution method*
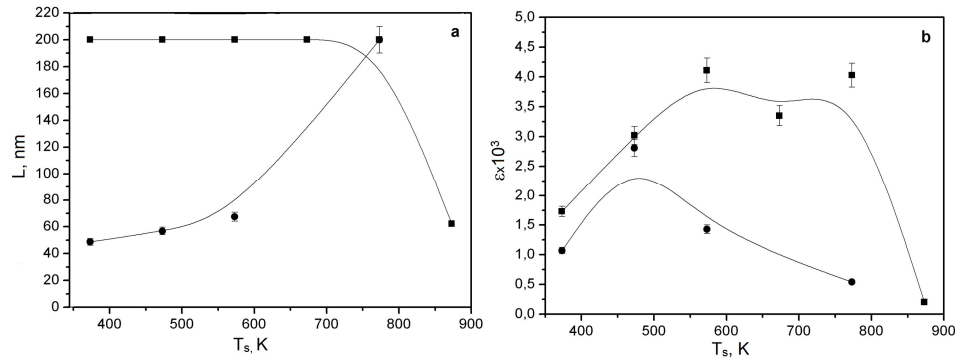
Fig. 18 − *Influence of substrate temperature T_s on SDS size L (a) and mirodeformation level ε (b) of CdSe films in directions (002) (●) and (100) (■)*

As Figure 18 a shows the L-T_s dependence in films with hexagonal structure has another view than in films with cubic phase. Crystallites of wurtzite phase of low-temperature condensates compiled of sub-grains that were near to cylindrical form and elongated in the direction f c crystallography axis. The height of these cylinders, $L_{(002)}$ ~ 200 nm (more values are non-physic [91-94]), in low-temperature condensates (T_s = 373 K), several times exceeded their diameter $L_{(100)}$ ~ 49 nm. An increase of the condensation temperature led to an increase in the cylinder's diameter up to $L_{(100)}$ = 200 nm in films obtained at T_s = 773 K. At the same time, their height decreased to 62 nm. It may be explained by the formation in these stacked layers of fault dislocations analogous to cubic structure films [83].
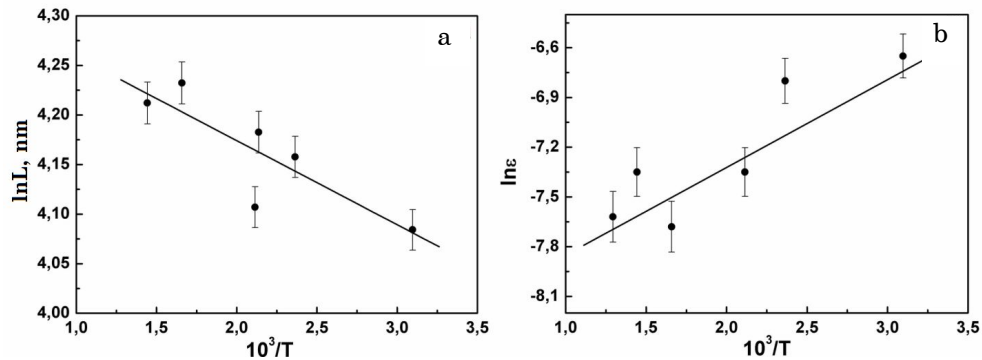
Microdeformation level in CdSe films essentially depends on the measured direction. So, microdeformations in the direction parallel to c crystallographic axis ($\varepsilon_{(002)}$ = (1.73-4.11)·10^{-3}) in general were 2-3 times bigger than in the perpendicular direction to this axis ($\varepsilon_{(100)}$ = (0.54-2.81)·10^{-3}). The dependence of in both directions was similar; the microdeformation value increased at first as the substrate temperature increased, after that it rapidly decreased for the high-temperature condensates (Fig. 18 b) [86, 88].

Determining the values of microdeformations and using the well-known ratio $\sigma = E\varepsilon$, the microstress level in chalcogenide films was evaluated (Table 5) [78, 82] using the values of Young modulus presented in [7, 16, 17]. The obtained values of σ for cubic ZnTe films are presented in Table 5. It was estimated that microstress level in ZnTe films varied in the range of σ = (20-83) MPa. Maximal microstress values (σ = (20-83) MPa) by size were considerably (3-5 times) smaller than that determined by the X-ray method (σ = (231-407) MPa) in electrodeposited ZnTe films in Ref. [99]. The SDS size in investigated films was near to that estimated in layers obtained by electrodeposition method (L = (44.7-78.0) nm). At the same time, this size was 2-3 times smaller than in films deposited by vacuum condensation L = (13.8-16.5) nm (101). As shown in Refs. [78, 81, 83, 85], this tendency was typical for all II-VI compounds films deposited in quasi-closed volume (CSS).

Table 5 − *Microstresses and dislocations density in ZnTe films*

T_s,К	(hkl)	L,nm	$\varepsilon\,10^3$	σ,MPa	$\rho_L, 10^{-13}$, lin/m^2	$\rho_\varepsilon, 10^{-13}$, lin/m^2	$\rho, 10^{-13}$, lin/m^2
charge	(111)-(222)	37.54	1.19	76.16	212.9	18.3	31.2
	(200)-(400)	75.21	1.07	68.48	53.0	19.7	16.2
323	(111)-(222)	59.39	1.29	82.56	85.1	21.5	21.4
	(200)-(400)	94.25	0.33	21.12	33.8	1.9	3.98
423	(111)-(222)	63.93	1.11	71.04	73.4	15.9	17.1
	(200)-(400)	48.65	0.42	26.88	126.8	3.0	9.8
468	(111)-(222)	65.54	0.43	27.52	69.8	2.4	6.5
	(200)-(400)	70.65	0.79	50.56	60.1	10.7	12.7
473	(111)-(222)	60.76	0.64	40.96	81.3	5.3	10.4
	(200)-(400)	-	-				
603	(111)-(222)	68.87	0.46	29.44	63.3	2.7	6.6
	(200)-(400)	75.98	0.51	32.64	51.9	4.5	7.6
693	(111)-(222)	67.50	0.64	40.96	65.8	5.3	9.3
	(200)-(400)	69.34	0.46	29.44	62.4	3.6	7.5
773	(111)-(222)	62.07	0.49	31.36	77.9	3.1	7.8

Thus, the results of investigations of the substructure of chalcogenide films obtained by CSS show that these films are structurally better than the films obtained by open vacuum evaporation method and some other methods. In Fig. 19 are presented values of ZnTe films' substructure reduced in co-ordinates $\ln L$ - $10^3 / T_s$ ($\ln\sigma$ - $10^3 / T_s$). The Figure shows that the data are well-approximated by straight line. The processes that determine the degree of dispersion of substructure elements and microdeformation level in the thin films were thermally activated [78, 81]. The slope of the line determines the corresponding activation energies. These energies were considerably smaller than self-diffusion energy of components in three-dimensional zinc telluride (ΔE = 2.7; 3.8 eV) [12]. This corresponds to atoms migrations onto the film's surface, which leads to disordering. This conclusion also applies to other chalcogenide compounds.

Fig. 19 − *Activation dependence of SDS sizes L (a) and microdeformation level ε (b) of ZnTe films to the substrate temperature T_s*

It is well-known that blocks sub-grains of different materials are formed by dislocations situated onto their boundaries with simultaneous dislocations situated inside blocks, which leads to microdeformations. One may estimate the average dislocation density in chalcogenide films by a microdeformation value ε and SDS size L. In Refs. [81, 83, 85] the authors used expressions presented in [96, 97, 99].

The results of dislocations density measurements of SDS in ZnTe films are given in Table 5. Investigated chalcogenide films characterized by low (see, for example (100), where $\rho = (6.3\text{-}16.6)\cdot10\cdot14$ lin/m^2) dislocations density and dependence ρ - T_s describes by curve with minimum. Measurement show that the dislocations are generally concentrated on the SDS boundaries. Crystalline volume is practically dislocations-free. On the average, one internal dislocation limps to 10 blocks. Such peculiarities of dislocation density were also observed by authors [81, 83, 85] in other chalcogenides films. In Fig. 20 is presented the dependence of dislocation density inside SDS, on their boundaries, and full value/throughout the volume in CdTe films vs. the substrate temperature [85].
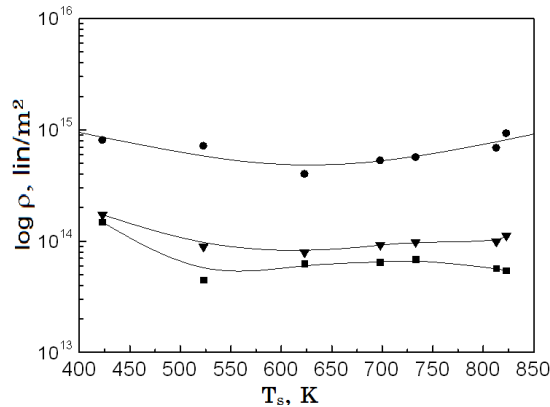

Fig. 20 − *Dislocations density inside SDS (●), on their boundaries (▼) and full value (■) in CdTe films versus the substrate temperature T_s*

The determination of SDS sizes by the Hall method and by the three-fold convolution typically give $L_{(h00)} > L_{(hhh)}$. This can be explained as follows: SDS is really non-equiaxial or their sizes in direction perpendicular to crystallographic planes (111) are less than in direction perpendicular to (200) or SDS sizes are equiaxial which correspond to reflections of (hhh) planes, that adding SFD [91-96].

Accepting the equality of SDS and the widening of (111) and (222) lines connected with the presence of SFD, it may be used to measure the sum of deformation and grown defects concentration using the ratio presented in [81, 83, 95, 96]. Results of α measuring in zinc telluride films were presented in Table 3 and Fig. 21.

Fig. 21 shows the decrease of general stacking fault dislocations density on increasing the substrate temperature from 0.67 % ($T_s = 323$ K) to 0.04 % ($T_s = 693$ K). Their largest number (1.43 %) was observed in charge [78, 81]. These values are considerably smaller than those determined in ZnTe films, obtained by electrochemical deposition for solution temperatures $T = (303\text{-}363)$ K ($\alpha = (1.5\text{-}8.5)\%$) [99].
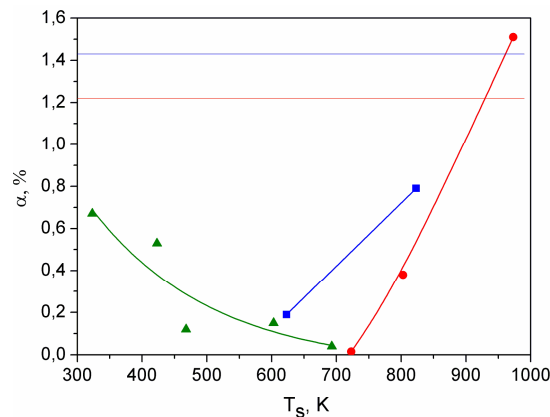
Fig. 21 *− SFD concentration dependence α in chalcogenide films from the substrate temperature T_s. ZnTe (▲), CdTe (■), ZnS (●). Straight lines marked a defects concentration in charge*

Simultaneously, as in the above investigated films, in the electrochemically deposited films it was observed that a decreasing of SFD density occurs as the temperature of synthesizing layers increases. These results are well-correlated with the thermodynamic sphalerite and wurtzite phases of this compound [12, 21]. An increase of T_s leads to increasing stability of cubic zinc telluride, which lowers the alternation of planes (111), and accordingly decreases the stacking fault dislocations density.

A reverse tendency is observed in ZnS films (CdTe). An increase of T_s in these materials monitored an increase of SFD. It may be explained by an increase of the hexagonal phase stability at high substrate temperatures and by acceleration of violation alternate probability of close-packed planes.

3. CONCLUSIONS

It was established that the physical peculiarities of the II-VI compounds lead to high defect concentration, existing of the metastable phases, and considerable deviation from the stoichiometry in obtained films. It was determined that grain boundaries, coherent scattering domain, dislocation, and native point defects have strong effect on the film's properties. The basic requirements for the structural and substructural properties of the thin films suitable for the devices manufactoring have been defined.

The methods of the II-VI thin films deposition were considered. The close-spaced vacuum sublimation method is considered as one of the most promising technique for chalcogenide films deposition. The structural peculiarities of thin films obtained by the close-spaced vacuum sublimation were studied. The influence of growth conditions on the structural and substructural properties such as phase compositions, texture, and grain size, stacking faults concentration, micro deformation levels and coherent domain size were analyzed. The growth conditions of the thin films with optimal parameters for the devices manufacturing have been determined.

REFERENCES

1. S.M. Sze, K.K. Ng, *Physics of semiconductor devices* (New Jersey: John Wiley and Sons: 2007).
2. J.P. Colinge, C.A. Colinge, *Physics of semiconductor devices* (New York: Springer Science+Business Media, Inc.: 2006).
3. B.G. Y. Kluwer, *Semiconductor materials. An Introduction to Basic Principles* (New York: Academic/Plenum Publishers: 2003).
4. K. Takahashi, A. Yoshikawa, A. Sandhu, W. Bandgap *Semiconductors. Fundamental Properties and Modern Photonic and Electronic Devices* (Berlin Heidelberg New York: Springer: 2007).
5. A.N. Georgobiani, *Phizika soedininij A_2B_6* (Moscow: Nauka: 1986) (in Russian).
6. A.N. Georgobiani, *UFN* **113, 129** (1974) (in Russian).
7. S. Kasap, P. Capper, *The Springer Handbook of Electronic and Photonic Materials* (Berlin: Springer: 2007).
8. B.V. Grinev, V.D. Ryzhikov, V.P. Seminozhenko, *Scintillation detectors and radiation systems on their base* (Kyiv: Naukova Dumka: 2007) (in Russian).
9. D.V. Korbutyak, S.V. Melnichuk, *Cadmium telluride: impurity-defects states and detector properties* (Kyiv: Ivan Fedorov: 2000) (in Ukrainian).
10. N.N. Berchenko, V.E. Krevs, V.G. Sredin, *Semiconductor solid solutions and their application: Reference tables* (Moskow: Voenizdat: 1982) (in Russian).
11. M. Ohring, *The materials science of thin films* (New York:Academic press: 1992).
12. I.P. Kalinkin, V.B. Aleskovskij, A.V. Simashkevich, *A_2B_6 epitaxial films compounds* (Leningrad: publishing LGU: 1978) (in Russian).
13. A. Farenbrook, R. Biube, *Solar cells theory and practice* (Moscow: Energoatomizdat: 1987) (in Russian).
14. P.A. Panchekha, *Functional materials* **7, 261** (2000).
15. P.A. Panchekha, O.G. Alaverdova, V.I. Gnidash, *UFZh* **45 (1), 75** (2000) (in Russian).
16. R.N. Bhargava, *Properties of wide-bandgap II-VI Semiconductor* (London: INSPEC: 1997).
17. S. Adachi, P. Capper, *Properties of group - IV, III−V and II−VI semiconductors* (New York: John Wiley & Sons: 2005).
18. Yu.V. Bochkov, A.N. Georgobiani, Z.P. Ilyuchina, B.N. Levonovich, N.V. Serdyuk, *Short reports on physics* **8**, 22 (1983) (in Russian).
19. B.N. Levonovich, *Thesis D. Sci. in technical academic degree competition* (Moscow: NIIMV: 2010) (in Russian).
20. M.P. Shackolskaja, *Crystallographia* (Moscow: Vysshaja shkola: 1984) (in Russian).
21. N.K. Morozova, V.A. Kuznetsov, *Zinc Sulfide. Obtain and optical properties* (Moscow: Nauka: 1987) (in Russian).
22. R. Grill, A. Zappettini, *Progr. Cryst. Growth Ch.* **48, 209** (2004).
23. P. Skeath, I. Lindau, C.Y. Sut, W.E. Spicer, *Phys. Rev. B* **28, 7051** (1983).
24. C.J. Panchal, M.S. Desai, V.A. Kheraj, K.J. Patel, N. Padha, *Semicond. Sci. Technol.* **23, 015003** (2008).
25. N.M. Shah, J.R. Ray, M.S. Desai, C.J. Panchal, *J. Optoelectron. Adv. M.* **12, 2052** (2010).
26. C.J. Panchal, *Indian. J. Phys.* **79, 1269** (2005).
27. N.G. Patel, C.J. Panchal, P.G. Patel, K.K. Makhija, S.S. Patel, *Cryst. Res. Technol.* **29, 247** (1994).
28. N.G. Patel, C.J. Panchal, K.K. Makhija, *Cryst. Res. Technol.* **29, 1013** (1994).
29. H.F. Matare, *Solid State Electron.* **22, 651** (1978).
30. H.F. Matare, *J. Appl. Phys.* **56, 2605** (1984).
31. К.M. Doshchanov, *PhTP* **32**(6), 690 (1998) (in Russian).

32. R.L. Petritz, *Phys.Rev.* **104,** 1508 (1956).
33. J.Y.W. Seto, *J. Appl. Phys.* **46,** 5247 (1975).
34. M. Lopez, J. Espinos, F. Martin, et al., *J. Cryst. Growth* **285,** 66 (2005).
35. T.A. Gessert, A.R. Mason, R.C. Reed, et al., *J. Electr. Mat.* **24,** 1443 (1995).
36. L. Shao, K. Chang, H. Hwang, *Appl. Surf. Science* **212,** 305 (2003).
37. Q. Liu, M. Guobing, A. Jianping, *Appl. Surf. Science* **254,** 5711 (2008).
38. J. Cheng, D. Fan, H. Wang [et al.], *Semicond. Sci. Technol.* **18,** 676 (2003).
39. V.B. Patil, D.S. Sutrave, G.S. Shahane, L.P. Deshmukh, *Thin Solid Films* **401,** 35 (2001).
40. J.P. Enriquez, X. Mathew, *Sol. Energy Mat.* **81,** 363 (2004).
41. A.S. Arico, D. Silvestro, P.L. Antonucci et al., *Adv. Perform. Mater.* **4,** 115 (1997).
42. A.V. Kokate, U.B. Suryavanshi, C.H. Bhosale, *Sol. Energy* **80,** 156 (2006).
43. N.J.S. Kissinger, M. Jayachandran, K. Perumal, C.S. Raja, *Bull. Mater. Sci.* **30,** 547 (2007).
44. A. Erlacher, A. Lukaszew, H. Jaeger, et al., *Surf. Science* **600,** 3762 (2006).
45. K. Sarmah, R. Sarma, H.L. Das, *Chalcogenide Lett.* **5,** 153 (2008).
46. S. Venkatachalam, Y.L. Jeychandran, P. Sureskumar, et al., *Mater. Charact.* **58,** 794 (2007).
47. L. Feng, D. Mao, J. Tang, et al., *J. Electron. Mater.* **25,** 1422 (1996).
48. A. Ali, N. Abbas Shah, A. Maqsood, *Sol. State Electron.* **52,** 205 (2008).
49. A. Lopez-Otero, *Thin Solid Films* **49,** 3 (1978).
50. D. Franta, I. Ohlidal, P. Klapetek, et al., *Thin Solid Films* **468,** 193 (2004).
51. K.H. Lee, J.H. Jung, T.W. Kim, H.S. Lee, H.L. Park, *Appl. Surf. Science* **253,** 8470 (2007).
52. P. Paiano, P. Prete, N. Lovergine, et al., *Cryst. Res. Technol.* **40,** 1011 (2005).
53. Y.P.V. Subbaiah, P. Prathap, K.T. Ramakrishna Reddy, *Appl. Surf. Sci.* **253,** 2409 (2006).
54. P. Prathap, Y.P.V. Subbaiah, K.T. Ramakrishna Reddy, R.W. Miles, *J. Phys. D: Appl. Phys.* **40,** 5275 (2007).
55. Y.P.V. Subbaiah, P. Prathap, K.T. Ramakrishna Reddy, *J. Phys.: Condens. Matter* **20,** 035205 (2008).
56. P. Prathap, N. Revathi, Y.P.V. Subbaiah, K.T. Ramakrishna Reddy, *Solid State Sci.* **11,** 224 (2009).
57. M.E. Hernandez-Torres, R. Silva-Gonzalez, G. Casarrubias-Segura, J.M. Gracia-Jimenez, *Sol. Energ. Mater.* **90,** 2241 (2006).
58. G.G. Rusu, *J. Optoelectron. Adv. M.* **8,** 931 (2006).
59. N. Abbas Shah, A. Ali, Z. Ali, et al., *J. Cryst. Growth* **284,** 477 (2005).
60. F. Shang, J. Ji-Kang, R. Wu, Y.-F. Zheng, Y.F. Sun, *Powder Diffr.* **23,** 31 (2008).
61. J. Luschitz, K. Lakus-Wollny, A. Klein, et al., *Thin Solid Films* **515,** 5814 (2007).
62. U. Alver, E. Bacaksiz, E. Yanmaz, *J. Alloys Compd.* **456,** 6 (2008).
63. Y.P.V. Subbaiah, P. Pratap, M. Device, *Physca B* **365,** 240 (2005).
64. G.I. Rusu, M. Diciu, C. Pirghie, E.M. Popa, *Appl. Surf. Sci.* **253,** 9500 (2007).
65. G.I. Rusu, M.E. Popa, G.G. Rusu, *Appl. Surf. Sci.* **218,** 222 (2003).
66. S. Armstrong, P.K. Datta, R.W. Miles, *Thin Solid Films* **403,** 126 (2002).
67. G.I. Rusu, P. Prepelita, N. Apetroaei, et al., *J. Optoelectron. Adv. M.* **7,** 829 (2005).
68. G.I. Rusu, P. Prepelita, R.S. Rusu, et al., *J. Optoelectron. Adv. M.* **8,** 922 (2006).
69. G.G. Rusu, *J. Optoelectron. Adv. M.* **8,** 931 (2006).
70. C. Baban, G.I. Rusu, P. Prepelita, *J. Optoelectron. Adv. M.* **7,** 817 (2005).
71. C. Baban, M. Caraman, G.I. Rusu, *J. Optoelectron. Adv. M.* **8,** 917 (2006).
72. S. Velumani, X. Mathew, P.J. Sebastian, *J. Mater. Sci. Lett.* **22,** 25 (2003).
73. S. Seto, S. Yamada, K. Suzuki, *Sol. Energ. Mat.* **67,** 167 (2001).
74. J. Takahashi, K. Mochizuki, K. Hitomi, et al., *J. Cryst. Growth* **269,** 419 (2004).

75. S.M. Danilchenko, T.G. Kalinichenko, M.M. Kolesnyk B.A. Mishchenko, A.S. Opanasyuk, *Visnyk SumDU. Seriya: fizyka, matematyka, mechanika* **1, 115** (2007) (in Ukrainian).
76. S.M. Danilchenko, M.M. Kolesnyk, D.I. Kurbatov, T.G. Kalinichenko, A.S. Opanasyuk, *FHTT* **9, 343** (2008) (in Ukrainian).
77. D.I. Kurbatov, S.M. Danilchenko, A.S. Opanasyuk, N.M. Opanasyuk, *Visnyk Lvivs'kogo universytetu, Seriya fizychna* **42, 108** (2008) (in Ukrainian).
78. M.M. Kolesnyk, S.M. Danilchenko, A.S. Opanasyuk, N.M. Opanasyuk, *Visnyk SumDU Seriya: fizyka, matematyka, mechanika* **2, 90** (2008) (in Ukrainian).
79. D. Kurbatov, V. Denisenko, A. Opanasyuk, A. Kramchenkov, M. Zaharets, *Semicond. Phys., Quant. Electr. Optoelectr.* **11, 252** (2008).
80. A.G. Balogh, S.M. Duvanov, D.I. Kurbatov, A.S. Opanasyuk, *Photoelectronics* **17**, 134 (2008).
81. D. Kurbatov, V. Kosyak, M. Kolesnyk, A. Opanasyuk, S. Danilchenko, *Integr. Ferroelectr.* **103, 32** (2009).
82. D. Kurbatov, M. Kolesnyk, A. Opanasyuk, V. Loboda, *Semicond. Phys., Quant. Electr. Optoelectr.* **12, 35** (2009).
83. D. Kurbatov, H. Khlyap, A. Opanasyuk, *phys. status solidi A* **206**, 1549 (2009).
84. V.V. Starikov, M.M. Ivashchenko, A.S. Opanasyuk, V.L. Perevertaylo, *J. Nano-Electron. Phys.* **1** No4, **119** (2009).
85. V.V. Kosyak, A.S. Opanasyuk, P.M. Bukivskij, Yu.P. Gnatenko, *J. Cryst. Growth* **312**, 1726 (2010).
86. M.M. Ivashchenko, A.S. Opanasyuk, S.M. Danilchenko, T.G. Kalinichenko, V.L. Perevertaylo, *FHTT* **11, 349** (2010).
87. M.M. Ivashchenko, A.S. Opanasyuk, S.M. Danilchenko, *Functional Materials* (in press).
88. M.M. Ivashchenko, A.S. Opanasyuk, N.M. Opanasyuk, S.M. Danilchenko, V.V. Starikov, *Semicond. Phys., Quant. Electr. Optoelectr.* (in press).
89. *Selected powder diffraction data for education straining* (Search manual and data cards) − (USA: International Centre for diffraction data: 1988).
90. Y. Yan, M. Al-Jassim, K. Jones, et al., *Appl. Phys. Lett.* **77, 1461** (2000).
91. L.I. Mirkin *X-ray structural analysis. Obtain and measurement of X-ray grams: Reference book* (Moscow: Nauka: 1976) (in Russian).
92. Ya.S. Umanskij, Yu.A. Skakov, A.N. Ivanov, L.N. Rastorgujev *Crystallography, X-ray graph and electronic microscopy* (Moscow: Metallurgija,: 1982) (in Russian).
93. B.E. Warren *X-ray Diffraction* (New York: Dover: 1990).
94. D.K. Bowen, K. Brian *Tanner X-Ray Metrology in Semiconductor Manufacturing* (London: Taylor & Francis Group: 2006).
95. L.S. Palatnik *Structure and physical properties of solid state.* (Kyiv.: Vyssha shkola: 1983) (in Russian).
96. L.S. Palatnik, M.Ya Fuks, V.M. Kosevich *Mechanism of self-formation and substructure of condensed films* (Moscow: Nauka: 1972) (in Russian).
97. A.S. Kagan, L.M. Syshlyannikova, A.P. Unikel, *Zavodskaja laboratorija* **46** (10), 903 (1980).
98. S.N. Danilchenko, O.G. Kukharenko, C. Moseke, *Cryst. Res. Technol.* **37, 1234** (2002).
99. T. Mahalingam, V.S. John, G. Ravi, *Cryst. Res. Technol.* **37, 329** (2002).